

The Placement of Lateral Regions in 1D MTR Fuel Lattice Cell Models

S. Day and W.J. Garland
McMaster University
September 1997

Abstract

Small experimental test reactors came to the forefront of the nuclear industry in the early development period of the 1950's and 1960's. Detailed analysis of plate-type fuel was done at the time with the constraints of the existing computer power and available codes. Since then the focus, in Canada and the United States, has shifted towards pin-type fuel currently used in newer research facilities and power reactors. However, recent operational and licensing issues at the McMaster Nuclear Reactor (MNR) have led to a renewed interest in characterization of these plate-type fuels.

The current industry standard lattice code, WIMS-AECL, is restricted to infinite-slab geometry for plate-fuel. Detailed models using this code and a similar lattice code, DRAGON, are presented and compared to the more simplistic models developed in the late 1970's and 1980's as part of the IAEA research reactor core conversion studies. Specifically, the extending of the lattice cell geometry and the inclusion of peripheral structural material is considered. A brief methodology for plate-fuel lattice cell analysis is also presented and discrepancies between the two lattice codes are discussed. This work is currently in progress.

I. Introduction

The present study was motivated by the current conversion of the McMaster Nuclear Reactor (MNR) core from HEU to LEU fuel. A subsequent upgrade in the code infrastructure for the facility is underway.

Part of the code center upgrade is the development of a more sophisticated series of lattice cell models for the representative sections of the MNR core. In the initial stages of our modeling we not only realized that there was a distinct lack of recent literature on advanced MTR plate fuel lattice modeling but also that available literature exists in a fragmented state [1-6].

The last readily available literature on plate-fuel modeling seems to be that associated with research reactor core conversion studies amassed by the IAEA in the late 1970's and early 1980's [1,2]. Since then, however, the enormous strides in computer resources have provided the ability to expand lattice cell modeling techniques and although this has been done [3] we are not aware of any detailed examination of the changes.

The studies of the 1980's were generally limited to few group, few region, one dimensional slab geometries [7-10]. Presently it is not only possible to increase the number of energy groups from ~5 to on the order of 90 but also possible to explicitly model many more material regions. However, since it is a one-dimensional representation, the question is raised: how should the peripheral structural materials be included in the model, if at all? This study is interested in investigating whether there is a noticeable impact and how large an effect there is by switching from a simple few

region model to a more realistic explicit geometry.

It is also hoped to present a methodology for analyzing plate-fuel lattice models which will be useful for future work. The two lattice cell codes, WIMS-AECL and DRAGON, were used in this analysis and the discrepancies between the two lattice codes are also presented and discussed.

II. Code Description

The two lattice codes used in this study were the AECL version of WIMS, WIMS-AECL [11,12] and DRAGON [13], developed at École Polytechnique, Montreal, Canada. WIMS-AECL is the current industry standard lattice code whereas DRAGON is being viewed as the eventual successor.

The WIMS-AECL lattice code contains a one-dimensional infinite-slab geometry option which is most relevant to modeling plate-type fuel as in MNR. Although DRAGON has 2D and 3D Cartesian geometry options, the 1D infinite slab model was examined as a comparison to the WIMS-AECL models. This is a work in progress at the present time since the DRAGON 2D models are not available for comparison. Therefore, the simple 1-plate model as used in the research reactor conversion studies of the 1980's is used as the reference calculation.

Both codes used the ENDF/B-V cross section library and solved the transport equation in the full 89 groups using collision probability methods. In all cases, leakage was not included in the model which will facilitate further comparison with future Monte Carlo models. The codes were executed on an HP Workstation. Output from both codes (Tape16 binary file for WIMS) was processed using a series of in-house Fortran, PERL and Matlab scripts with calculations and plotting done in Matlab V.4.

In the WIMS-AECL models the peripheral material was defined as "moderator" for spectrum assignment purposes in the self-shielding routine.

III. Geometries Studied

There are two types of fuel elements in the present MNR core. The first is the 18-plate element (~62.5 cm x 8.001 cm x 7.610 cm) which contains 16 fueled plates and two similar solid aluminum "dummy" plates (one on each end of the element). The plates are 0.127 cm thick (0.0381 cm clad, 0.0508 cm fuel meat) and 6.657 cm wide with the fuel meat only extending 6.23 cm. The plates are held between two aluminum sideplates (0.47625 cm x 8.001 cm). Light water is pumped in a downward direction through coolant gaps of 0.300 cm thickness which extend fully between the sideplates. The second type of fuel element is the 10-plate fuel (~62.5 cm x 8.0264 cm x 7.610 cm). This element contains 10 fueled plates and no "dummy" plates. Each plate has slightly thicker cladding (0.0508 cm) for a thickness of 0.1524 cm. The coolant gaps are also larger at a thickness of 0.635 cm. The dimensions and fuel compositions are summarized in Table 1 and the 18-plate fuel element is illustrated in Figure 1.

Each element in the MNR core is fixed in position by an aluminum grid plate on the bottom of the

core. This grid plate defines a spacing between elements which is filled with light water. Therefore, each element effectively has a surrounding region of light water, between the fuel structure and the cell boundary, which should be considered as part of the lattice cell. The grid dimensions for each element are 8.10006 cm x 7.7089 cm.

Table 1: Fuel Element Specifications for MNR [14,15]

	18-Plate	10-Plate
fuel type	UAlx, 22% wt U, 93% enriched	
grid spacing (cm)	8.10006 x 7.7089	
active plate width (cm)	6.23	
fuel plate thickness (cm)	0.0508	0.0508
Al clad thickness (cm)	0.0381	0.0508
coolant gap thickness (cm)	0.300	0.635
Volume %		
fuel	8.11	5.07
Al clad	12.16	10.14
coolant	47.89	63.36
Extra H ₂ O (moderator)	15.57	8.15
Extra Al	16.27	13.29

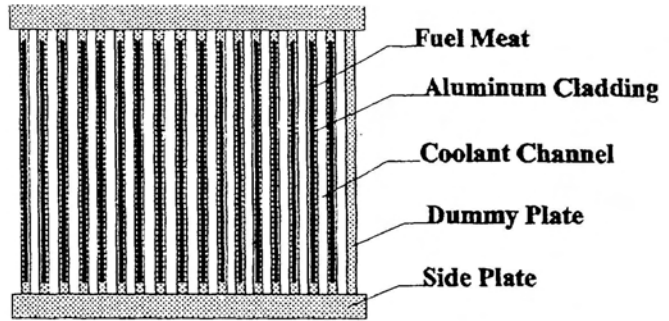


Figure 1: MTR 18-plate fuel element cross section

IV. Analysis Methodology

The variation of a series of parameters were examined when comparing lattice code models. Most of the analysis deals with cell averaged quantities, specifically the infinite multiplication factor, k_{inf} ; the spectrum index, r ,

$$r \equiv \frac{\Phi_1}{\Phi_2} \quad (1)$$

where Φ_1 is the fast flux defined as that from 4 eV \rightarrow 10 MeV, and Φ_2 is the thermal flux defined as that below 4 eV; and the 2-group cell averaged absorption and ν^* fission cross sections (energy group division also at 4 eV). The percent of the total cell absorption in each bulk material (*ie.*, fuel, clad, coolant, and peripheral regions) is also presented to indicate the relative importance placed on the peripheral materials.

In addition to these cell averaged parameters, we also examined some local quantities. The spectrum index as well as the ratio of the ν^* fission to absorption reaction rates in each fuel plate was

determined. As part of the code comparison the regional flux profiles were also examined.

V. Lattice Cell Modeling Approaches

In the two lattice codes (for the 1D slab geometry) the fuel plates and respective coolant gaps are defined as infinite 1D slabs from a reflective centerline to a reflective outer boundary. Since the plate and coolant gap thicknesses are small in comparison to their widths (ratios of 49 and 20 respectively for the 18-plate case) then it may be thought that ignoring the peripheral structures may be a good approximation. Without any of the peripheral or “extra regions” the fuel element can be modeled simply as 1 plate with surrounding coolant channels being repeated by the reflective boundary conditions. This is shown in Figure 2 and is used as the reference case in this study.

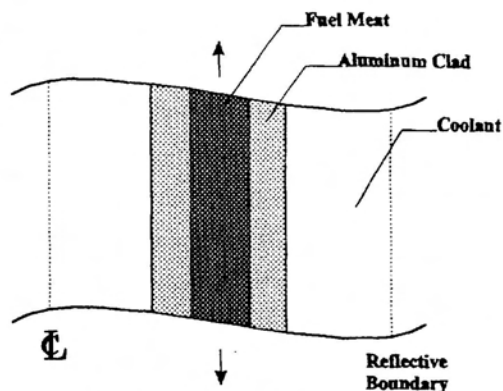


Figure 2: 1-Plate simple geometry model of fuel element. Extra regions can be added as additional slabs on centerline and reflective outer boundary.

However, if these extra regions are to be included, the question is: how should they be incorporated into the model? More specifically, the extra regions are defined as the material extending beyond the width of the fuel meat, termed “lateral extra regions” (eg., the plate and coolant gap ends, sideplates and surrounding water) and the material beyond the last fuel plates, termed “normal extra regions” (eg., the dummy plate and adjacent water in the 18-plate model). These are more clearly shown in Figure 3.

In order to determine the importance of these “extra regions” a series of more elaborate models were constructed. As an initial step, the 1-plate model as shown in Figure 2 was modified so that the proportion of extra material applicable to 1 fuel plate was included as additional slabs on the centerline and outer boundary. More detailed models were then constructed which explicitly modeled the fuel plate region of the element (ie., the regions within the fueled width of each plate) from the centerline through the normal extra regions. The question still remained: in what position

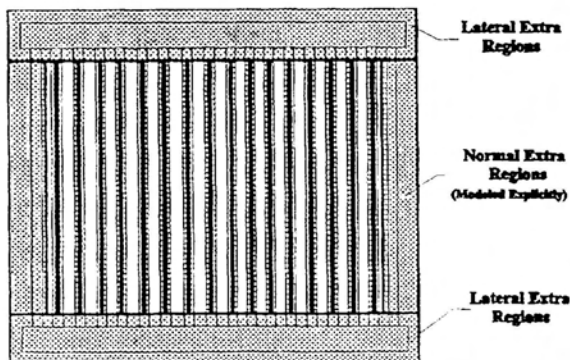


Figure 3: Extra region definition in MTR 18-plate fuel element.

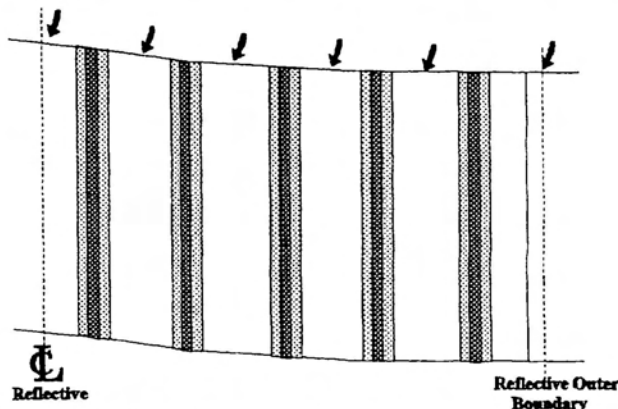


Figure 4: Placement of lateral extra regions in 10-plate fuel model indicated by arrows at applicable distances from centerline.

should the lateral extra regions be incorporated? Each fuel plate “sees” a section of this lateral material so we proceeded by adding extra slabs of the lateral Al/water in the center of the coolant gaps between each fuel plate and on the outer boundary of the model. This is shown in Figure 4. Models were constructed with 0, 25, 50, 75 and 100% of the lateral extra material placed on the outer boundary.

VI. Results and Discussion

The inclusion of the extra regions seems to be quite significant. This is not surprising as the extra light water accounts for 15.57% and 8.15% of the cell volumes in the 18-plate and 10-plate cases respectively (25.53% and 11.40% of the total water volume in the respective cases). Even though their importance may be somewhat reduced by the fact that they are peripheral regions, the tight dimensions with respect to the average mean free path makes this characteristic secondary.

The inclusion of the extra regions results in a significant lowering of the spectrum index, and a reduction in k_{inf} on the order of 95-140 mk (WIMS-AECL) and 77-107 mk (DRAGON) for the 18-plate fuel, and 84-93 mk (WIMS-AECL) and 84-93 mk (DRAGON) for the 10-plate model. This is reflected in the lowering of the cell averaged cross section values on the order of 30% for the 18-plate case and 17% for the 10-plate case. The results are shown in Tables 2-5.

Table 2: WIMS-AECL 18-Plate Fuel Model Cell Quantities and Differences

Model	K_{inf}	Σ_{a1} (cm-1)	Σ_{a2} (cm-1)	$\nu\Sigma_{f1}$ (cm-1)	$\nu\Sigma_{f2}$ (cm-1)
1ps (reference)	1.746700	0.002714	0.083162	0.003722	0.147655
difference	mk	%	%	%	%
1p	-95.6	-27.1	-23.8	-29.9	-28.2
hc-0	-110.8	-27.8	-25.8	-30.6	-30.8
hc-25	-110.8	-27.7	-26.8	-30.5	-32.0
hc-50	-116.7	-27.6	-27.8	-30.4	-33.2
hc-75	-123.3	-27.5	-28.9	-30.2	-34.5
hc-100	-138.0	-27.4	-30.0	-30.1	-35.9

(legend: K_{inf} = infinite multiplication factor, Σ_{ax} = group x macroscopic absorption cross section, $\nu\Sigma_{fx}$ = group x macroscopic ν *fission cross section, 1ps = 1-plate simple model (no extra regions), 1p = 1-plate model with extra regions, hc-0 = explicit half cell model with 0% of the extra material on the reflective outer cell boundary (similar nomenclature for the remaining entries 25, 50, 75, 100))

Table 3: DRAGON 18-Plate Fuel Model Cell Quantities and Differences

Model	Kinf	Σ_{a1} (cm-1)	Σ_{a2} (cm-1)	$\nu\Sigma_{f1}$ (cm-1)	$\nu\Sigma_{f2}$ (cm-1)
1ps (reference)	1.814383	0.002838	0.065155	0.003849	0.122615
difference	mk	%	%	%	%
1p	-83.7	-27.9	-16.2	-30.7	-21.2
hc-0	-77.0	-27.5	-21.8	-30.2	-25.9
hc-25	-82.6	-27.5	-22.6	-30.2	-26.9
hc-50	-89.4	-27.5	-23.6	-30.3	-28.2
hc-75	-97.5	-27.5	-24.7	-30.3	-29.6
hc-100	-106.4	-27.6	-25.9	-30.3	-31.1

Table 4: WMS-AECL 10-Plate Fuel Model Cell Quantities and Differences

Model	Kinf	Σ_{a1} (cm-1)	Σ_{a2} (cm-1)	$\nu\Sigma_{f1}$ (cm-1)	$\nu\Sigma_{f2}$ (cm-1)
1ps (reference)	1.547979	0.001626	0.057997	0.002075	0.090401
difference	mk	%	%	%	%
1p	-84.1	-16.6	-16.4	-19.7	-21.0
hc-0	-84.2	-16.9	-16.4	-19.9	-21.0
hc-25	-84.2	-16.8	-16.5	-19.9	-21.2
hc-50	-85.4	-16.8	-16.8	-19.8	-21.6
hc-75	-87.2	-16.7	-17.1	-19.7	-22.0
hc-100	-92.6	-16.6	-17.6	-19.6	-22.6

Table 5: DRAGON 10-Plate Fuel Model Cell Quantities and Differences

Model	Kinf	Σ_{a1} (cm-1)	Σ_{a2} (cm-1)	$\nu\Sigma_{f1}$ (cm-1)	$\nu\Sigma_{f2}$ (cm-1)
1ps (reference)	1.725115	0.001702	0.047059	0.002144	0.082815
difference	mk	%	%	%	%
1p	-88.5	-17.7	-14.1	-20.4	-18.8
hc-0	—	—	—	—	—
hc-25	-89.7	-17.7	-14.3	-20.4	-19.0
hc-50	-92.5	-17.6	-14.6	-20.4	-19.5
hc-75	-96.8	-17.5	-15.1	-20.4	-20.2
hc-100	-102.1	-17.5	-15.6	-20.4	-21.0

(legend: Kinf = infinite multiplication factor, Σ_{ax} = group x macroscopic absorption cross section, $\nu\Sigma_{fx}$ = group x macroscopic nu*fission cross section, 1ps = 1-plate simple model (no extra regions), 1p = 1-plate model with extra regions, hc-0 = explicit half cell model with 0% of the extra material on the reflective outer cell boundary (similar nomenclature for the remaining entries 25, 50, 75, 100))

The position of the lateral extra regions has a smaller but still noticeable effect on the cell quantities. When comparing the 1-plate and half-cell models, the multiplication factor shows a further lowering of 15.2-42.4 mk/ 0.1-8.5 mk (WIMS-AECL) and differences between 6.7-22.7 mk/ 0.1-8.5 mk (DRAGON) for the 18-plate / 10-plate models. The fast group cross sections are not significantly effected whereas the thermal group results are lowered by 6-10% for the 18-plate case and only 1-2% for the 10-plate case. These are probably the most significant results as they would be the quantities extracted for use in the subsequent core code analysis.

The results for the fast group constants are not surprising as the neutron mean free path is much longer so local material region effects would tend to be smeared over the entire lattice cell. The cell averaged thermal group absorption and $\nu \cdot \text{fission}$ cross sections are lowered as more of the lateral extra material is placed on the outer boundary of the geometry (and subsequently less is placed between the fuel plates). This thermal group reduction in cross section is consistent with the shift in percent cell absorption shown in Tables 6-9.

A word of caution must be added when comparing the multiplication factor and percent absorption results between the 1-plate and multiple-plate models. Comparing the two showed significant differences. This may be due in part to the effective placement of the normal extra regions between the plates in the 1-plate model as opposed to the actual position on the outer boundary of the cell in the multiple plate model. The effect was larger for the 18-plate fuel which has a larger normal region contribution. There is also a difference between adding the extra regions between the plates (1-plate model) and on the outer boundary (multiple-plate models) The DRAGON code seems to show a larger offset in the numbers.

Table 6: Percent Absorption in bulk materials for WIMS-AECL 18-plate fuel model

Model	coolant	clad	fuel	normal extra	lateral extra	total extra
1ps	11.29	1.80	86.91	—	—	—
1p	10.64	1.68	81.78	2.66	3.24	5.90
hc-0	10.55	1.66	81.02	3.52	3.25	6.77
hc-25	10.51	1.66	80.73	3.55	3.55	7.10
hc-50	10.47	1.65	80.42	3.59	3.88	7.47
hc-75	10.42	1.65	80.07	3.61	4.25	7.86
hc-100	10.37	1.64	79.70	3.64	4.66	9.29

(legend: 1ps = 1-plate simple model (no extra regions), 1p = 1-plate model with extra regions, hc-0 = explicit half cell model with 0% of the extra material on the reflective outer cell boundary (similar nomenclature for the remaining entries 25, 50, 75, 100))

Table 7: Percent Absorption in bulk materials for DRAGON 18-plate fuel model

Model	coolant	clad	fuel	normal extra	lateral extra	total extra
1ps	6.16	1.86	91.98	—	—	—
1p	5.72	1.73	86.52	2.71	3.32	6.03
hc-0	5.75	1.74	87.16	1.98	3.36	5.34
hc-25	5.74	1.74	86.89	2.03	3.60	5.63
hc-50	5.72	1.73	86.56	2.07	3.92	5.99
hc-75	5.70	1.73	86.16	2.11	4.30	6.41
hc-100	5.68	1.72	85.72	2.13	4.75	6.88

Table 8: Percent Absorption in bulk materials for WIMS-AECL 10-plate fuel model

Model	coolant	clad	fuel	normal extra	lateral extra	total extra
1ps	21.72	2.10	76.19	—	—	—
1p	20.52	1.97	71.99	0.75	4.77	5.51
hc-0	20.52	1.97	71.98	0.78	4.75	5.52
hc-25	20.51	1.97	71.93	0.79	4.81	5.60
hc-50	20.48	1.97	71.84	0.80	4.91	5.71
hc-75	20.45	1.97	71.72	0.81	5.06	5.86
hc-100	20.41	1.96	71.57	0.81	5.24	6.06

Table 9: Percent Absorption in bulk materials for DRAGON 10-plate fuel model

Model	coolant	clad	fuel	normal extra	lateral extra	total extra
1ps	12.03	2.27	85.70	—	—	—
1p	11.32	2.14	81.06	0.41	5.07	5.48
hc-0	—	—	—	—	—	—
hc-25	11.32	2.14	81.00	0.43	5.11	5.54
hc-50	11.30	2.13	80.87	0.44	5.26	5.70
hc-75	11.27	2.13	80.66	0.45	5.49	5.94
hc-100	11.24	2.12	80.41	0.45	5.77	6.23

(legend: 1ps = 1-plate simple model (no extra regions), 1p = 1-plate model with extra regions, hc-0 = explicit half cell model with 0% of the extra material on the reflective outer cell boundary (similar nomenclature for the remaining entries 25, 50, 75, 100))

As more of the lateral moderating material is placed on the outer boundary of the cell, more of the thermal flux is concentrated in this region rather than in the more reactive fuel plate region of the cell therefore placing more emphasis on the smaller water absorption cross sections as compared to the higher fuel absorption cross sections. The increased extra region absorption also explains the reduction in the multiplication factor since, although the fission rate relative to the absorption rate

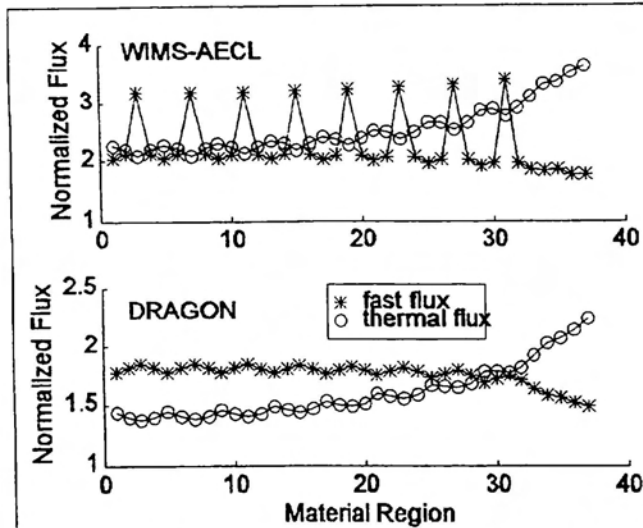


Figure 5: Regional flux profile for 18-plate 1D fuel model. Fast flux is group 1 of 4 and thermal flux is group 4 of 4. Note: fast flux peaks in fuel regions.

in the fuel is increased in the outer fuel plates, this effect is not enough to counteract the increased absorption.

The final point considered was the discrepancies between the two codes. Both contained identical geometry and material input, utilized the same cross section library, and every effort was made to keep the solution scheme consistent between the two. It is obvious from the above data that the DRAGON code gives a much more reactive lattice cell with significantly reduced absorption in the coolant and increased absorption in the fuel meat. Although these discrepancies exist, both codes show the same trends in the cell averaged and regional

parameters previously discussed.

Upon closer examination of the two models a noticeable difference in the regional flux profile was noticed. This is shown in Figure 5. The WIMS-AECL data shows the fast flux peaking higher in the outer fuel plates whereas the DRAGON code shows an opposite trend with the fast-flux-peaking becoming smaller from the center plate to the outer plates. On the one hand, the WIMS-AECL results may look reasonable. Since the thermal flux is increasing in the outer fuel plates, the presence of more thermal neutrons would cause more fissions and therefore result in a higher fast flux contribution. However, one must consider the dimensions of the fuel element. Because the interplate dimensions are quite small as compared with a typical mean free path of the neutrons, especially the fast neutrons, a global flux shape may dominate rather than the local plate flux shape which would be consistent with the DRAGON results.

These fundamental differences in the two codes may justify further exploration. Preliminary results from similar Monte Carlo studies indicate a closer agreement with the cell averaged numbers of the WIMS-AECL code but a flux shape similar to the DRAGON results.

VII. Conclusions

The data collected in this study will hopefully serve as a useful reference for further plate-fuel lattice code work. The analysis methodology outlined herein and parameters chosen for analysis seem appropriate for determining the inner workings of the lattice code model in question.

Our results indicate that the most important aspect of the 1D lattice cell model is the inclusion of the peripheral regions, being more important in the 18-plate case as opposed to the 10-plate case due to the volume fraction of these regions and the coolant gap characteristics of the fuel geometry. The effect on 2-group cell averaged cross sections was on the order of 15-30%. Once these extra regions are included in the model there is some effect in positioning these regions, mostly evident in the

thermal range cross sections.

Further work is underway to compare the 1D results to those from a 2D explicit DRAGON model. This may facilitate a recipe for placement of the lateral regions in a 1D lattice cell model. We plan to use the lattice cell results in a 3D diffusion core code model of MNR in order to determine the lattice cell variations' effect on the final system results.

The two lattice codes, WIMS-AECL and DRAGON, showed some inconsistencies which should be further explored. A comparison to similar Monte Carlo models is underway.

VIII. References

1. "Research Reactor Core Conversion from the use of Highly Enriched Uranium to the use of Low Enriched Uranium Fuels Guidebook", IAEA-TECDOC-233, International Atomic Energy Agency, 1980
2. F. Woloch, and G. Stimpfl-Abele, "Review of International Atomic Energy Agency Benchmark Calculations on the Conversion of Research and Test Reactors", *Nuclear Technology*, Vol. 58, August 1982, pp. 196-202
3. R.J. Ellis, S.G. King, and J.J. Orchard, "A Validation of WIMS-AECL/3DDT Against SPERT-1B Reactivity Measurements", RTB-TN-017 RTB-010.11, Atomic Energy of Canada Whiteshell Laboratories, April 1994
4. R.J. Ellis, AECL-WL, Personal Communication.
5. J.V. Donnelly, AECL-SHPK, Personal Communication.
6. R.J. Stamm'ler, and M.J. Abbate, Methods of Steady-State Reactor Physics in Nuclear Design, Academic Press, 1988.
7. E. Yilmaz, and B.G. Jones, "Selection and Benchmarking of Computer Codes for Research Reactor Core Conversions", *Nuclear Technology*, Vol. 64, Jan. 1984.
8. M. Straka, and L. Covington, "Study of Neutron Physics: Conversion of the University of Missouri-Rolla Reactor to Low Enriched Fuel", *Trans. of the ANS*; v. 55, 1987.
9. T. Aldemir, J.W. Talnagi and D.W. Miller, "Low-Enriched Uranium Conversion/Power Upgrade of the Ohio State University Research Reactor", *Nuclear Technology*, Vol. 86, Sept. 1989.
10. S.M.R. Nejat, "Preliminary Neutronics Calculations for Conversion of the Tehran Research Reactor Core from HEU to LEU Fuel", *Nuclear Technology*, Vol. 103, Aug. 1993.
11. J. Griffiths, "WIMS-AECL Users Manual", RC-1176, COG-94-52, Atomic Energy of Canada Ltd., March 1994.
12. R.J. Askew, F.U. Fayers, and P.B. Kemshell, "A General Description of the Lattice Code WIMS", *J. Br. Nucl. Energy Soc.*, v. 5, pp. 564-585, Oct. 1966.
13. G. Marleau, A. Hébert and R. Roy, "A User's Guide for DRAGON", IGE-174 Rev.1, Institut de génie nucléaire, Département de génie mécanique, École Polytechnique de Montréal, March 1996.
14. H.S. Basha, "Dimensions for the MNR Standard Fuel Assembly", MNR-QA-SF-1 Rev.0, Oct. 1996.
15. MNR blueprints, No. 1605D2 Grid Plate Spacer, No. 1322.081 18-Plate Fuel Element, available at MNR.